On-the-fly molecular dynamics study of the excited-state branching reaction of α-methyl-*cis*-stilbene

Takuro Tsutsumi,[a] Yu Harabuchi,[b,c] Rina Yamamoto,[a] Satoshi Maeda,[b] and Tetsuya Taketsugu[a,b,*]

[a]*Graduate School of Chemical Sciences and Engineering, Hokkaido University, N13-W8, Kita-ku, Sapporo 060-8628, Japan*

[b]*Department of Chemistry, Faculty of Science, Hokkaido University, N10-W8, Kita-ku, Sapporo 060-0810, Japan*

[c]*Precursory Research for Embryonic Science and Technology (PRESTO), Japan Science and Technology Agency (JST), Saitama 332-0012, Japan.*

ABSTRACT

The branching reaction of α-methyl-*cis*-stilbene (*cis*-mSB) into its *trans*-mSB and 4a,4b-dihydrophenanthrene (DHP) forms upon ππ* excitation was examined theoretically by exploring the excited-state potential energy surface and using on-the-fly molecular dynamics simulations at the spin-flip time-dependent density functional theory (SF-TDDFT) level of theory. The branching ratio of trajectories was calculated as DHP:*twist* = 11:29, where *twist* denotes a mid-region between the *cis*-form and *trans*-form, indicating that the *trans*-mSB is a dominant product. The branching mechanism was analyzed by comparison with the corresponding theoretical studies on stilbene (SB) and 1,1'-dimethyl-stilbene (dmSB). The present computations elucidate the origin of variations in the branching ratio in the photoreactions of *cis*-SB, *cis*-mSB, and *cis*-dmSB. We also found that, because of loss of the slow component of the decay to the ground state, *cis*-mSB shows a faster decay rate to the ground state than *cis*-SB and *cis*-dmSB.

KEYWORDS

stilbene, excited-state dynamics, reaction pathways, on-the-fly MD

AUTHOR INFORMATION

Corresponding Author: E-mail: take@sci.hokudai.ac.jp (T. Taketsugu)

Notes: The authors declare no competing financial interest.

Graphical abstract:

I. Introduction

It is now recognised that the conical intersection (CI) of the potential energy surfaces (PESs) of the adiabatic electronic states plays a significant role in photoreactions [1–3]. Recent progress in theoretical chemistry has made it feasible to elucidate the mechanism and dynamics of photoreactions involving a nonradiative decay through CIs by the highly sophisticated quantum chemical approaches [4–6], ab initio surface hopping molecular dynamics with the nonadiabatic coupling terms [7,8], and systematic exploration of minimum energy CI (MECI) structures based on the global reaction route mapping (GRRM) strategy [9–11]. A systematic search for low-lying MECIs enables the determination of the energetically favourable internal conversion paths from the Franck–Condon region. Recently, the difference of fluorescence quantum yields of aromatic molecules has been discussed based on the barrier heights along the internal conversion paths [12,13].

Stilbene (SB) is a typical molecule that shows *cis–trans* photoisomerisation about the central C=C bond on the ππ* excitation, and the photoisomerisation process of SB has been investigated by many experimental [14–25] and theoretical [26–32] studies. *trans*-SB has a planar geometry of C_{2h} symmetry, and the isomerization pathway in the ππ* excited state for leaving the fluorescent region accompanies a small barrier, and thus, the lifetime was reported to be relatively long (10 ~ >100 ps) [18,22]. On the other hand, ππ*-excited *cis*-SB exhibits ultrafast decay to the ground state with a lifetime of around 1.0 ps [20,21] *via* the CI points of the singlet excited-state (S_1) and ground-state (S_0) potential energy surfaces (PESs) in the *twist* region where the central C=C bond is twisted; this is known as the phantom state (P*) [15]. Theoretical studies on the decay mechanism of the ππ*-excited *cis*-SB have confirmed the twisting motion of the central C=C bond in the S_1 state, and this motion is known as the "hula-twist" [23]. Femtosecond Raman spectroscopy with quantum chemical calculations has clarified the initial nuclear dynamics of the ππ*-excited *cis*-SB based on the transit change of the vibrational spectra [24]. Femtosecond time-resolved fluorescence showed that the lifetime

of the excited *cis*-SB has two components at 0.23 and 1.2 ps [25].

It is known that ππ*-excited *cis*-SB has a by-product, 4a,4b-dihydrophenanthrene (DHP). The branching ratio of the products from ππ*-excited *cis*-SB has been reported to be *cis*:*trans*:DHP = 55:35:10 [16,17,19]. Thus, the dominant product is *trans*-SB. Minezawa and Gordon [29] employed a spin-flip time-dependent density functional theory (SF-TDDFT) method [33–35] to locate the geometries of the minima in the S_1 state, as well as minimum-energy conical intersection (MECI) points of the S_1 and S_0 states in the *twist* ($(S_1)_{twist\text{-min}}$ and $(S_1/S_0)_{twist}$) and DHP ($(S_1)_{DHP\text{-min}}$ and $(S_1/S_0)_{DHP}$) regions of the S_1-PES. It was also found that the photcyclisation is in competition with the photoisomerisation [29], which was later confirmed by a more sophisticated multireference method [30].

Harabuchi *et al.* [31] carried out reaction-path calculations on the S_1-PES and on-the-fly molecular dynamics (MD) simulations for the ππ*-excited *cis*-SB at the SF-TDDFT level of theory and discussed the reaction mechanism and dynamics. Along the steepest descent pathway starting from the Franck–Condon *cis*-structure, the two H atoms bound to the central C=C first move quickly so that each C-H-C_6H_5 fragment in SB becomes planar and the S_1-PES becomes very flat; then, the pathway becomes sharply curved toward the DHP-form. It was found that the pathway shows a bifurcation in a very flat region of the S_1-PES: one direction is toward the DHP region as the pathway itself indicates, whereas the other is toward the *twist* region with a very small activation barrier. The excited-state reaction path bifurcation can be regarded as an extension of the ground-state reaction path bifurcation [36,37]. The branching ratio from the on-the-fly MD simulations on the ππ*-excited *cis*-SB indicated that the dominant product is *trans*-SB (*trans*:DHP = 35:13), which is consistent with the experimental data. This result suggests the importance of dynamics in the photoreaction.

In 2012, Berndt *et al.* [38] reported an experimental study of the photoreactions of 1,1'-dimethylstilbene (dmSB) in solution, using transit-absorption spectra. It was reported that the peak at 600 nm, which corresponds to the absorption band of the *cis*-form in the S_1 state (CIS*)

decreases with a lifetime of 0.2 ps, which is shorter than the corresponding lifetime of *cis*-SB (0.92 ps), while the peak at 330 nm corresponding to the absorption band of the P* state shows a surprisingly long lifetime: 19 ps in hexane, which is much longer than the corresponding lifetime of *cis*-SB (1.2 ps) [38]. Harabuchi *et al.* [39] carried out theoretical computations of the excited-state PES and on-the-fly MD simulations for the reaction process of *cis*-dmSB in the S_1 state, and found that the long lifetime of the P* state in dmSB can be ascribed to the large geometrical difference between $(S_1)_{twist\text{-min}}$ and $(S_1/S_0)_{twist}$ in the *twist* region and that, in the case of the ππ*-excited *cis*-dmSB, the dominant product is not *trans*-dmSB but dmDHP. Very recently, Kokado *et al.* [40] examined the structural transformation of ππ*-excited tetraphenylethene, in which the four H atoms in ethylene are substituted by four phenyl rings, both experimentally and theoretically and proposed that the rotation about the central C=C bond is essential for the target process. The effect of substitution on the photoreaction process is a significant factor that determines the decay lifetime and quantum yield of photoisomerisation for stilbene derivatives, and, thus, theoretical examination of the excited-state reaction process for new substituted species should provide valuable insights.

Figure 1 shows the *cis*-, *trans*-, and DHP-forms of stilbene derivatives; by changing R^1 and R^2 to different groups, various stilbene derivatives can be obtained. In this study, we have chosen α-methyl-*cis*-stilbene (*cis*-mSB) as a target species, which should have a character between those of *cis*-SB and *cis*-dmSB, although only *cis*-mSB has asymmetric groups for R^1 and R^2. In the same way as previous studies on *cis*-SB and *cis*-dmSB, we examined the S_1-PES and on-the-fly MD simulations for the ππ* excited *cis*-mSB at the SF-TDDFT level of theory and examined the reaction pathways in the S_1-state, the branching ratio for products from MD simulations, and the decay lifetime to the ground state. Because there are no experimental studies on this species, our computations can be used as predictions for this new target molecule.

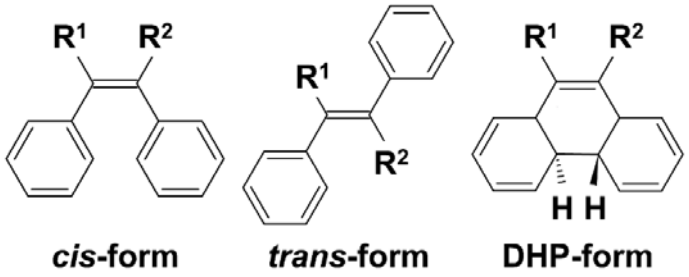

Figure 1. Three isomers of stilbene derivatives: stilbene for $^{1}R = {}^{2}R = H$; α-methyl-stilbene for ^{1}R = methyl group and $^{2}R = H$; 1,1'-dimethylstilbene for $^{1}R = {}^{2}R$ = methyl group.

II. Computational details

Geometry optimisations were performed on mSB at the SF-TDDFT level of theory to locate the minima in the S_0 and S_1 states (corresponding to *cis*-, *trans*-, *twist*-, and DHP-forms), the transition state (TS) structures that connect the DHP and *twist* regions in the S_1 state, and the S_1/S_0-MECIs in DHP and *twist* regions [33–35]. The obtained geometries were verified as minima or transition states by normal mode analysis. The intrinsic reaction coordinate (IRC) [36] was calculated from the S_1-TS to confirm the connectivity of the two minima in the DHP and *twist* regions. The steepest descent path in the S_1 state was calculated from the Franck–Condon (FC) structure in mass-weighted coordinates (referred to as the meta-IRC path). The SF-TDDFT calculations were performed with the BHHLYP functional and 6-31G(d) basis set using the GAMESS program [41], whereas all the minima, TSs, MECIs, IRCs, and meta-IRC paths were calculated by employing the GRRM14 program [42] with GAMESS. The branching plane update method [43] was used in geometry optimisation for the S_1/S_0-MECIs.

On-the-fly MD simulations were performed for the ππ*-excited *cis*-mSB at the SF-TDDFT level using the SPPR program [44]. To avoid mixed singlet and triplet states in SF-TDDFT calculations around the CI region along the trajectory, the T_{SF}-index method [10] was employed. The initial conditions for the on-the-fly MD simulations were determined by normal mode sampling of the ground state equilibrium geometry of *cis*-mSB. The atomic coordinates and velocities were generated randomly by adding an energy of kT to each normal mode under the Boltzmann distribution at 300 K. The time step was set to 0.2 fs, and 40 trajectories were calculated until the energy difference between the S_0 and S_1 states became less than 0.2 eV or the simulation time reached 1 ps.

III. Results and discussion

A. Geometries of minima, TSs, and S_1/S_0-MECIs

For mSB, we located four minima in the S_0 state ((S_0)$_{cis\text{-min}}$, (S_0)$_{DHP\text{-min}}$, (S_0)$_{trans1\text{-min}}$, and (S_0)$_{trans2\text{-min}}$), three minima in the S_1 state ((S_1)$_{DHP\text{-min}}$, (S_1)$_{twist1\text{-min}}$, and (S_1)$_{twist2\text{-min}}$), and one TS between (S_1)$_{DHP\text{-min}}$ and (S_1)$_{twist1\text{-min}}$ ((S_1)$_{TS}$). In the two *trans*-minima in the S_0 state, the two phenyl rings are deviated slightly from the central ethylenic plane by steric repulsion with the methyl ring, as is the case for dmSB [39], and the difference between these two structures is shown by the $d_{C1C2C4C6}$ dihedral angles (31.8° for (S_0)$_{trans1\text{-min}}$ and −39.8° for (S_0)$_{trans2\text{-min}}$). **Figure 2** shows the optimised geometries of these minima and the TS, as well as the energies of the S_0 and S_1 states relative to (S_0)$_{cis\text{-min}}$, $E(S_0)$ and $E(S_1)$, and four significant geometric parameters: r_{C5C6}, $d_{C3C1C2C4}$, $d_{H7C1C2C3}$, and $d_{C8C2C1C4}$ (r_{AB} denotes the interatomic distance of *A* and *B* atoms, and d_{ABCD} denotes the dihedral angle for *A*-*B*-*C*-*D* atoms); r_{C5C6} is a measure of the cyclisation from the *cis*-form to the DHP-form, and $d_{C3C1C2C4}$ is a measure of the *cis*-*trans* (or *cis*-*twist*) structural transformation; $d_{H7C1C2C3}$ and $d_{C8C2C1C4}$ represents the deformation of H7 and C8, respectively, from the central ethylenic planar part. The two *trans*-forms have almost the same energies which are very slightly lower than that of the *cis*-form (within 1 kcal/mol).

The central C=C part of (S_0)$_{DHP\text{-min}}$ shows an almost planar structure ($d_{C3C1C2C4}$ = −10.1°), whereas the corresponding dihedral angle becomes larger at (S_1)$_{DHP\text{-min}}$ ($d_{C3C1C2C4}$ = −20.6°). In the *twist* region in the S_1 state, two minima, (S_1)$_{twist1\text{-min}}$ and (S_1)$_{twist2\text{-min}}$, were found; the former has a pyramidal structure at H-C-phenyl (H-pyramidal) with $d_{H7C1C2C3}$ = −141.8°, and the latter has a pyramidal structure at CH_3-C-phenyl (Me-pyramidal) with $d_{C8C2C1C4}$ = −138.5°. (S_1)$_{twist2\text{-min}}$ is energetically higher than (S_1)$_{twist1\text{-min}}$ (92.5 *vs.* 85.5 kcal/mol) because of the repulsion of the methyl ring and phenyl ring. As shown in Fig. 2c, we also located a TS in the S_1 state, and verified that (S_1)$_{TS}$ connects (S_1)$_{DHP\text{-min}}$ and (S_1)$_{twist1\text{-min}}$ *via* IRC calculations. Thus, the molecule will prefer the H-pyramidal structure to the Me-pyramidal structure in the

twist region.

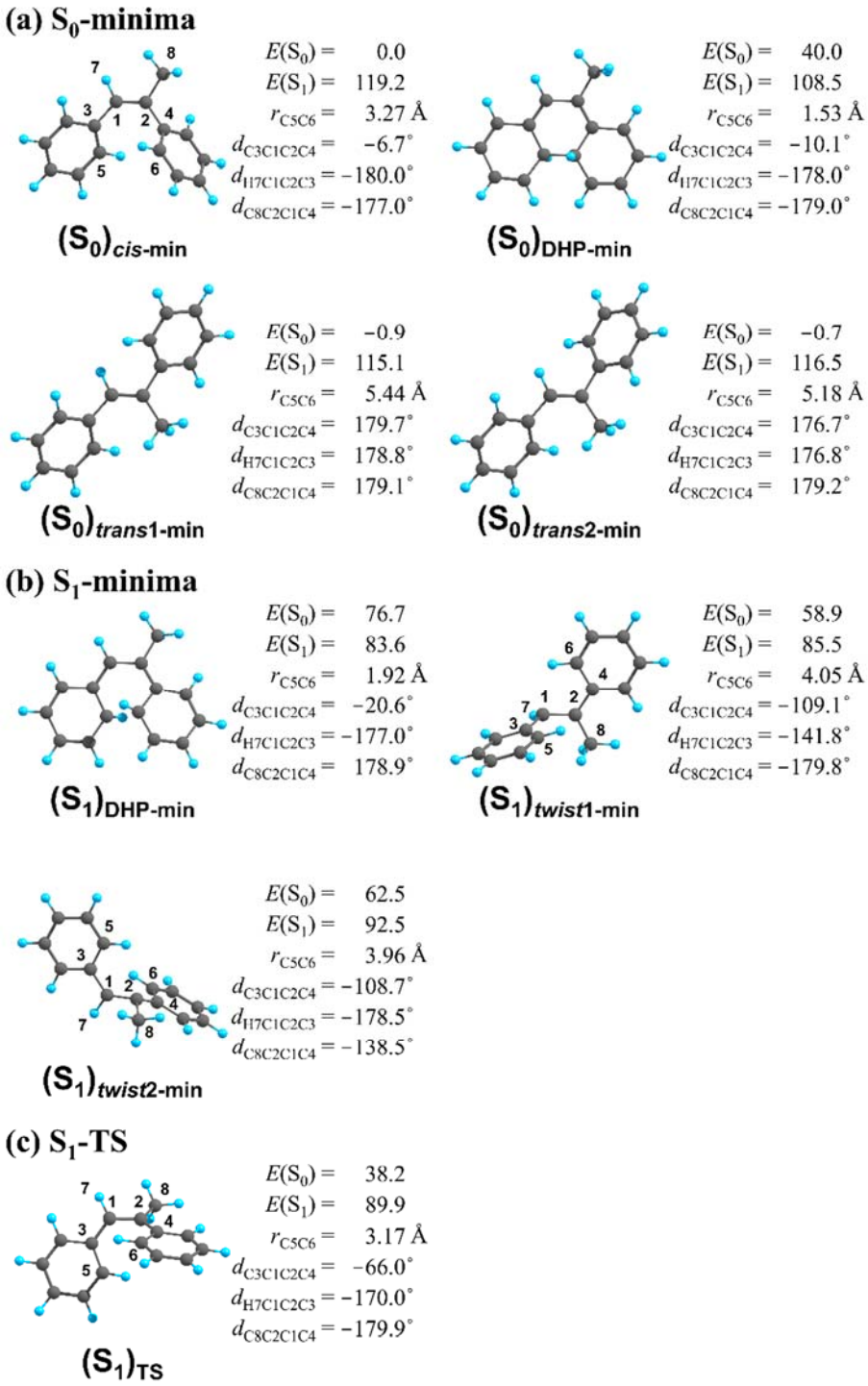

Figure 2. The optimised geometries of (a) the four minima in the S_0 state, (b) three minima in the S_1 state, and (c) one TS in the S_1 state for mSB. The energies of the S_0 and S_1 states relative to $(S_0)_{cis\text{-min}}$ (in kcal/mol) and significant geometrical parameters are also given.

Concerning the S_1/S_0-MECI structures, we located two structures in the DHP region and six structures in the *twist* region, as shown in **Fig. 3**. In the DHP region, $(S_1/S_0)_{DHP1}$ corresponds to the H-pyramidal structure ($d_{H7C1C2C3} = -164.7°$ and $d_{C8C2C1C4} = 178.8°$), while $(S_1/S_0)_{DHP2}$ corresponds to the Me-pyramidal structure ($d_{H7C1C2C3} = 177.8°$ and $d_{C8C2C1C4} = -160.8°$), although the pyramidal parts are close to the planar structure compared to the S_1-minima. $(S_1/S_0)_{DHP1}$ is more stable than $(S_1/S_0)_{DHP2}$ (85.9 *vs.* 92.1 kcal/mol) because of the steric repulsion between the methyl group and the phenyl ring in the Me-pyramidal structure. The $(S_1/S_0)_{DHP1}$ is energetically close to $(S_1)_{DHP\text{-}min}$ (83.6 kcal/mol), indicating that the molecule could easily relax to the ground state through $(S_1/S_0)_{DHP1}$. The six S_1/S_0-MECI structures in the *twist* region are given in the order of the relative energies. $(S_1/S_0)_{twist1}$ and $(S_1/S_0)_{twist3}$ correspond to the H-pyramidal structure, whereas $(S_1/S_0)_{twist2}$, $(S_1/S_0)_{twist4}$, $(S_1/S_0)_{twist5}$, and $(S_1/S_0)_{twist6}$ correspond to the Me-pyramidal structure. These structures can be further classified into the *trans*-type and *cis*-type according to the relative positions of two phenyl rings; $(S_1/S_0)_{twist1}$, $(S_1/S_0)_{twist2}$, and $(S_1/S_0)_{twist4}$ correspond to the twisted-*trans*-pyramidal structure, and $(S_1/S_0)_{twist3}$, $(S_1/S_0)_{twist5}$, and $(S_1/S_0)_{twist6}$ correspond to the twisted-*cis*-pyramidal structure. The latter twisted-*cis*-pyramidal-type MECI has not been reported previously. Taking into account these two classifications, the six S_1/S_0-MECI structures in the *twist* region can be classified into four types, *i.e.*, H-twisted-*trans*-pyramidal ($(S_1/S_0)_{twist1}$), H-twisted-*cis*-pyramidal ($(S_1/S_0)_{twist3}$), Me-twisted-*trans*-pyramidal ($(S_1/S_0)_{twist2}$, $(S_1/S_0)_{twist4}$), and Me-twisted-*cis*-pyramidal ($(S_1/S_0)_{twist5}$, $(S_1/S_0)_{twist6}$). The difference between $(S_1/S_0)_{twist2}$ and $(S_1/S_0)_{twist4}$ is the bond angle in the pyramidal part: a_{C1C2C4} is close to 90° in $(S_1/S_0)_{twist2}$, and a_{C1C2C8} is close to 90° in $(S_1/S_0)_{twist4}$. Similarly, a_{C1C2C4} is close to 90° in $(S_1/S_0)_{twist6}$, and a_{C1C2C8} is close to 90° in $(S_1/S_0)_{twist5}$. Similar geometrical features of the MECI structures were observed for SB and dmSB [31,39]. $(S_1/S_0)_{twist3}$ can also be classified by this viewpoint (a_{C2C1C7} is close to 90°), unlike $(S_1/S_0)_{twist1}$ (the smallest bond angle is 98.8°).

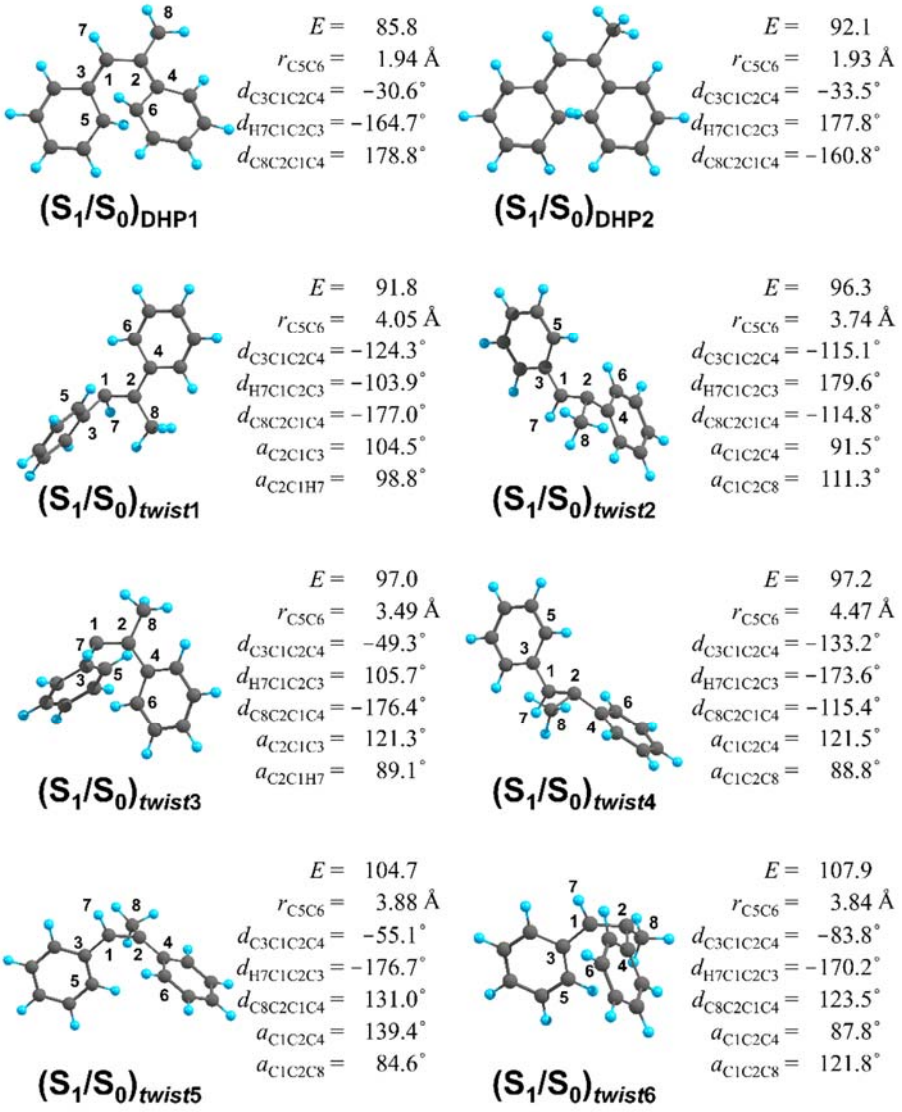

Figure 3. The optimised geometries of the calculated eight S_1/S_0-MECIs for mSB. The energy relative to $(S_0)_{cis\text{-min}}$ (E in kcal/mol) and significant geometrical parameters are also shown.

In the dynamics simulations, the molecule is expected to reach the energetically low-lying CI region. We performed meta-IRC calculations starting from the eight MECIs in the *twist* region, and verified that all the pathways reach $(S_1)_{twist1\text{-min}}$ or $(S_1)_{twist2\text{-min}}$ without a barrier, indicating that the energy level of each MECI can be used to judge whether the corresponding MECI is accessible by trajectories wandering around the S_1-minima.

B. Reaction pathways in the S_1 state

The ππ*-excited *cis*-mSB should move down the slope of the S_1-PES and branch into the DHP and *twist* regions. Following the previous studies on *cis*-SB [31] and *cis*-dmSB [39], we first examined the S_1-PES in the two-dimensional coordinate space spanned by r_{C5C6} (which characterises the transformation to the DHP) and $d_{C3C1C2C4}$ (which characterises the transformation to the *twist* form). **Figure 4** shows the positions of the stationary points in the S_0 and S_1 states and the S_1/S_0-MECIs, as well as the reaction pathways of the meta-IRC from the Franck-Condon *cis*-structure (red solid line) and the IRC between the DHP and *twist* minima (blue dotted line), in two-dimensional coordinate space for (a) mSB, (b) SB, and (c) dmSB. The H-pyramidal S_1/S_0-MECIs are indicated by blue cross marks, and the Me-pyramidal S_1/S_0-MECIs are indicated by green cross marks. As shown in Fig. 4, the DHP and *twist* regions are separated by a single TS for mSB and SB, whereas there are DHP, *cis*, and *twist* regions separated by two TSs, for dmSB. The meta-IRC path from the FC structure reaches the IRC pathway between $(S_1)_{DHP\text{-}min}$ and $(S_1)_{twist1\text{-}min}$, indicating a branched reaction pathway.

The profile of the meta-IRC route suggests that there is a preference for the DHP region over the *twist* region in all cases. In the case of SB, however, the direction of the meta-IRC path is toward the *twist* region before reaching the IRC between the DHP and *twist* minima as shown in Fig. 4b, and thus, the inertial force will push the molecule to the *twist* region. On the other hand, in the case of dmSB, the direction of the meta-IRC path is toward the DHP region from the start of the pathway, as shown in Fig. 4c, indicating that the DHP-form is expected as a major product. The case of mSB is between those of SB and dmSB, and the branching ratio over the DHP and *twist* regions will be sensitive to the dynamic effects in the same way as in the case of SB [31].

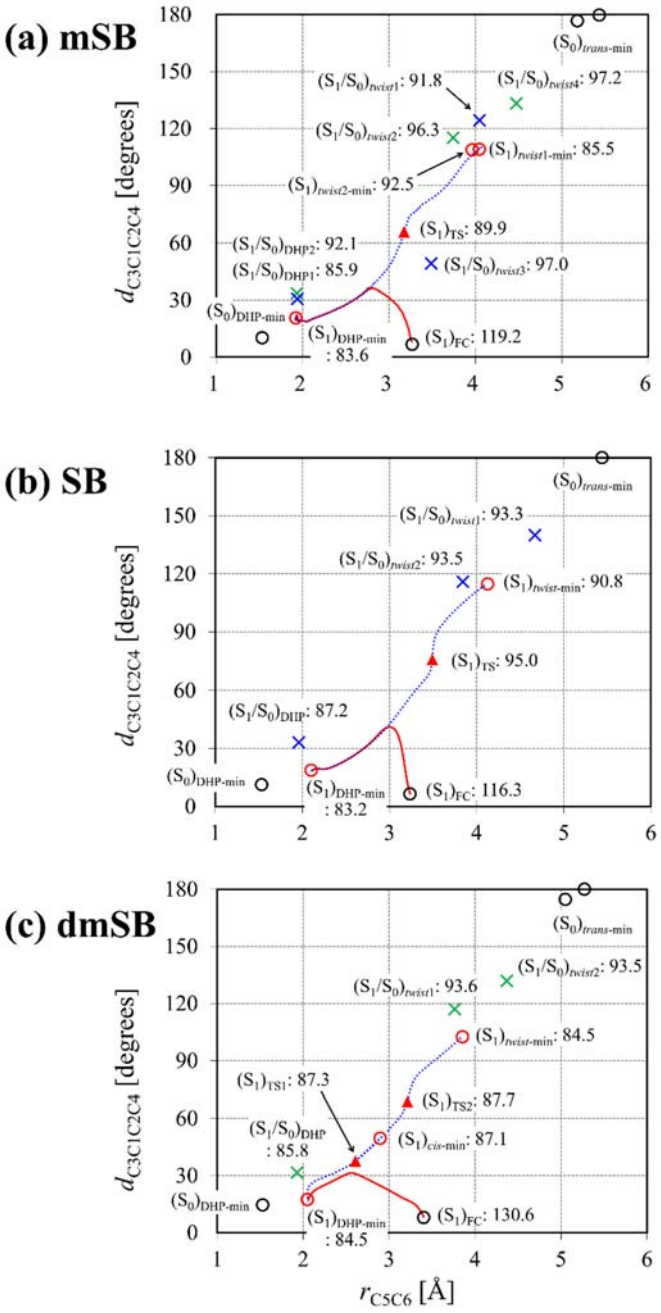

Figure 4. The minima, TSs, and MECI structures and the reaction pathways in the S_1 state for (a) mSB, (b) SB [31], and (c) dmSB [39] projected onto two-dimensional coordinate space in terms of r_{C5C6} and $d_{C3C1C2C4}$. The S_1-minima and S_1-TS are depicted by red circles and red triangles, respectively; the H-pyramidal S_1/S_0-MECIs are given by blue cross marks, and the Me-pyramidal S_1/S_0-MECIs are given by green cross marks. The S_0-minima are also given by black circles. The meta-IRC path from the FC point is denoted by a solid red line, and the IRC paths are denoted by a blue dotted line. The S_1 energies (in kcal/mol) relative to $(S_0)_{cis\text{-min}}$ are given for the respective structures.

Figure 5 shows the variations in the dihedral angles $d_{C3C1C2C4}$, $d_{R7C1C2C4}$, and $d_{R8C2C1C3}$ (R = H or C) and r_{C5C6} along the meta-IRC from the FC point of *cis*-form for (a) mSB, (b) SB, and (c) dmSB, where $d_{C3C1C2C4}$ (in red) corresponds to the rotational angle of two phenyl groups about the C=C bond, and $d_{R7C1C2C4}$ (in blue) and $d_{R8C2C1C3}$ (in green) correspond to the deviations in R7 and R8, respectively, with respect to the central ethylenic plane. In SB and dmSB, $d_{R7C1C2C4}$ and $d_{R8C2C1C3}$ have the same values along the meta-IRC pathway because of the C_2 symmetry. The $d_{C3C1C2C4}$ and a pair of $d_{R7C1C2C4}$ and $d_{R8C2C1C3}$ show a synchronous change where the former shows an increase from 10° to 40°, whereas the latter shows a decrease from 175° to 150°. The gradients of the change in these dihedral angles in the initial stage indicate that ππ*-exited *cis*-SB is promptly accelerated toward the twisted-form, whereas, in the case of ππ*-exited *cis*-dmSB, the corresponding acceleration is much smaller, and the ππ*-exited *cis*-mSB is the middle of *cis*-SB and *cis*-dmSB, which is consistent with the reaction route profiles in Fig. 4. The difference in the reaction path profile between *cis*-SB and *cis*-dmSB can be ascribed to the difference in the mass of the H and CH_3 groups in the central ethylenic part [39]. Actually, in the case of mSB, $d_{H7C1C2C4}$ decreases more rapidly than $d_{C8C2C1C3}$ as shown in Fig. 5a. The existence of H and CH_3 group in mSB will introduce mixed dynamics effects.

In Fig. 4, we note the energy difference between the S_1-minima and S_1/S_0-MECIs in the *twist* region. The most interesting feature of the ππ*-excited dmSB is the long lifetime of the P* state, and this was ascribed to the difference in the S_1-minimum and S_1/S_0-MECI structures, as well as a relatively large energy difference between these two structures [39]. In the case of mSB, all S_1-minima and S_1/S_0-MECI have a pyramidal structure, and the energy difference of the lowest S_1-minimum and S_1/S_0-MECI is 6.3 kcal/mol which is smaller than the dmSB case (9 kcal/mol) and larger than the SB case (3 kcal/mol). Therefore, the ππ*-excited *cis*-mSB will reach the S_1/S_0-CI structures in the *twist* region much faster than the dmSB case, although its excited-state lifetime should be longer than the SB case.

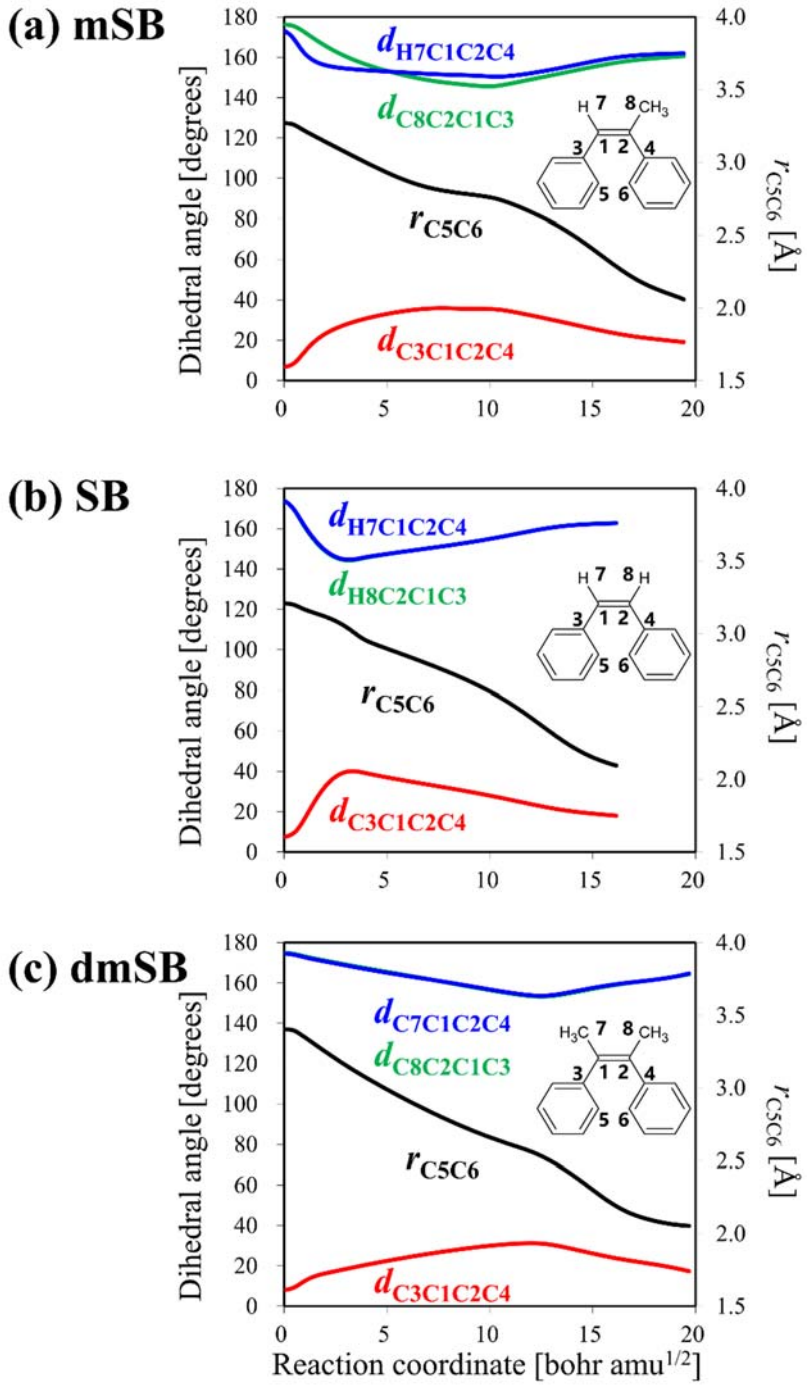

Figure 5. Variations in the dihedral angles and r_{C5C6} along the meta-IRC from the Franck-Condon structures for (a) *cis*-mSB, (b) *cis*-SB, and (c) *cis*-dmSB; $d_{C3C1C2C4}$ (in red) corresponds to the opening of two phenyl rings from *cis*- to *twist*-structure, $d_{R7C1C2C4}$ (in blue) corresponds to the motion of R7, and $d_{R8C2C1C3}$ (in green) corresponds to the motion of R8.

C. On-the-fly MD simulations

The dynamics of the ππ*-excited *cis*-mSB, showing the branched nature toward the DHP and *twist* regions on the S_1-PES, was examined by on-the-fly MD simulations at the SF-TDDFT level. In total, 40 trajectories were run from the FC region of the *cis*-form, in which 11 trajectories reach the DHP region while 29 trajectories reach the *twist* region, resulting in a DHP:*twist* branching ratio of 0.275:0.725. There is one exceptional trajectory that enters the *twist* region first, and then it moves to the DHP region later without reaching S_1/S_0-CIs in the *twist* region. In our previous studies, the branching ratio for DHP:*twist* was calculated as 0.26:0.74 for *cis*-SB [31] and 0.85:0.15 for *cis*-dmSB [39], and thus, the ratio for *cis*-mSB is very close to that for *cis*-SB. Only in the case of *cis*-dmSB are the terminal points of trajectories scattered mainly in the DHP region, which can be explained by the meta-IRC profile being directed toward the DHP-form from the start of the run [39]. In the case of *cis*-mSB, the meta-IRC profile and the position and energy of $(S_1)_{TS}$ suggest that there is a preference for the *twist* region over the DHP region in the dynamics.

During a total simulation time of 1.0 ps, nine trajectories among the 11 trajectories entering the DHP region reached the CI region in 364 fs on average, while 16 trajectories among the 29 trajectories entering the *twist* region reached the CI region in 635 fs on average. Thus, the trajectories entering the DHP region from the FC region can more easily reach the S_1/S_0-CI and hop to the ground state than those trajectories entering the *twist* region. **Figure 6** shows projections of four trajectories to the two-dimensional coordinate space, as examples: the trajectories entering the DHP region and reaching the CI region with (a) the shortest time (117 fs) and (b) the longest time (876 fs), and the trajectories entering the *twist* region and reaching the CI region with (c) the shortest time (390 fs) and (d) the longest time (979 fs). As shown in **Fig. 6c** and **6d**, the trajectories which finally entered the *twist* region wandered while in the region between $(S_1)_{DHP\text{-}min}$ and $(S_1)_{TS}$, leading to the relatively longer lifetime compared to the trajectories in the DHP region. We also analyzed the terminal CI points of nine trajectories in

the DHP region. Four terminal structures can be categorised as H-pyramidal CI (close to $(S_1/S_0)_{DHP1}$), and one terminal structure can be categorised as Me-pyramidal CI (close to $(S_1/S_0)_{DHP2}$). However, it is difficult to classify the other four structures into H-pyramidal or Me-pyramidal structures: ($d_{H7C1C2C3}$, $d_{C8C2C1C4}$) = (-177.7°, -173.2°), (-174.3°, -175.0°), (-170.0°, -173.2°), and (164.5°, -164.0°). In the case of the 16 trajectories that terminated in the *twist* region, the terminal CIs are all characterised as an H-twisted-*trans*-pyramidal structures corresponding to $(S_1/S_0)_{twist1}$.

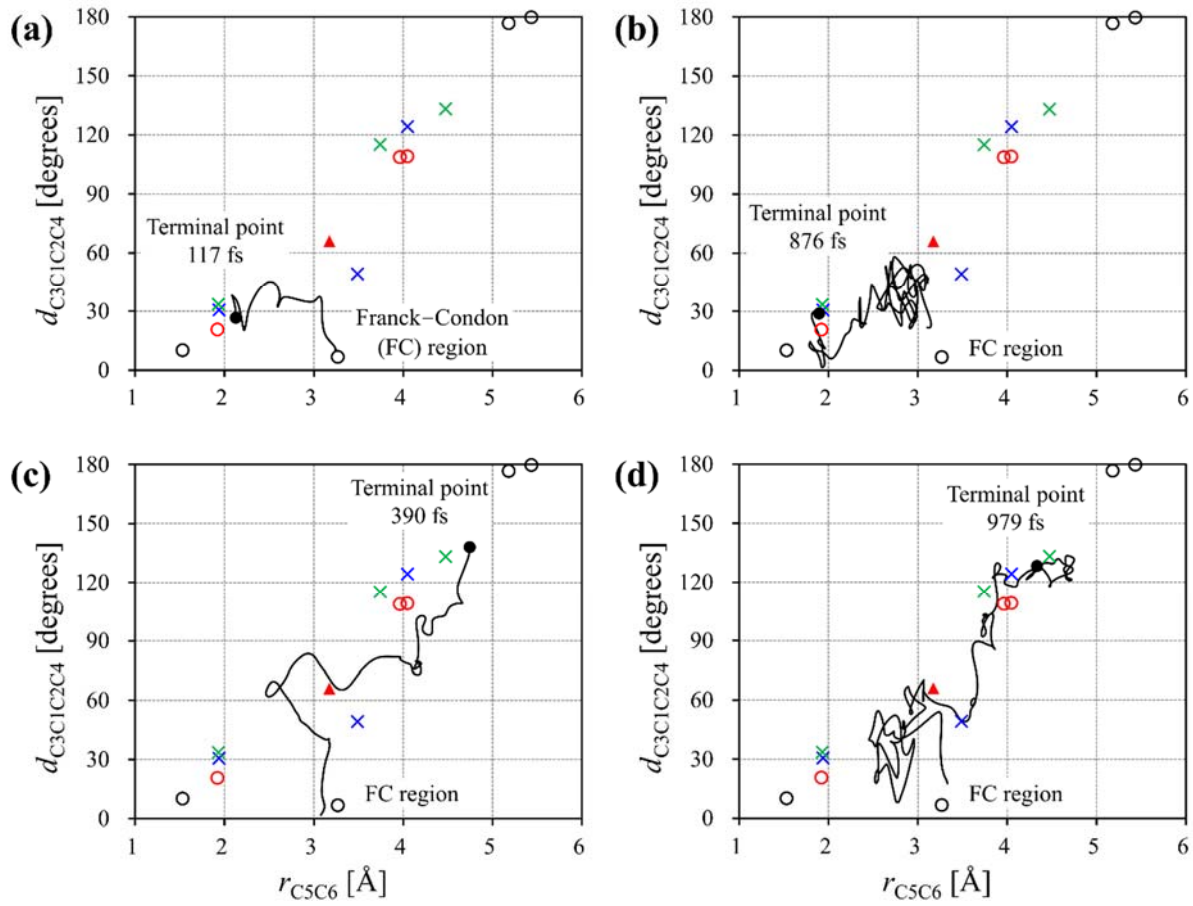

Figure 6. Four trajectories that start from the FC region of the *cis*-form and run on the S_1-PES: (a) one terminated at the CI in the DHP region with the shortest time; (b) one terminated at the CI in the DHP region with the longest time; (c) one terminated at the CI in the *twist* region with the shortest time; and (d) one terminated at the CI in the *twist* region with the longest time.

Figure 7 shows the decay of the S_1-population as a function of time calculated from on-the-fly MD simulations for (a) *cis*-mSB, (b) *cis*-SB [31], and (c) *cis*-dmSB [39], where all S_1 trajectories, those terminated in the DHP region, and those terminated in the *twist* region are plotted in black, red, and blue, respectively. Here, the "S_1-population" is defined as a ratio of the trajectories before reaching the crossing points of the S_0 and S_1 states. The trajectories in the *twist* region reached the CI more quickly in SB (Fig. 7b), whereas the trajectories in the DHP region reached the CI more quickly in dmSB (Fig. 7c). These results can be explained by the directions of the meta-IRC path from the FC region in the initial stages, as well as the geometrical and energy differences of the S_1-minimum and S_1/S_0-CI structures in the *twist* region for dmSB [39]. In the case of mSB, the trajectories in the DHP region reach the CI more quickly than in the *twist* region, as for dmSB, but the trajectories in the *twist* region reach the CI smoothly. In other words, *cis*-mSB has no long-lifetime component in the S_1 state, unlike the *cis*-SB and *cis*-dmSB cases. This feature of *cis*-mSB is ascribed to the initial direction of the meta-IRC, which is oriented between the *twist* (*cis*-SB) and DHP (*cis*-dmSB) regions. In the *twist* region, the decay rate for mSB is slightly longer than that for SB because the energy difference of S_1-minima and S_1/S_0-MECIs is larger for mSB than for SB. The present on-the-fly MD simulations demonstrate that the introduction of light (H) and relatively heavy (CH_3) fragments to the central part of the molecule tunes the lifetime and results in the disappearance of the slow component in the excited-state dynamics.

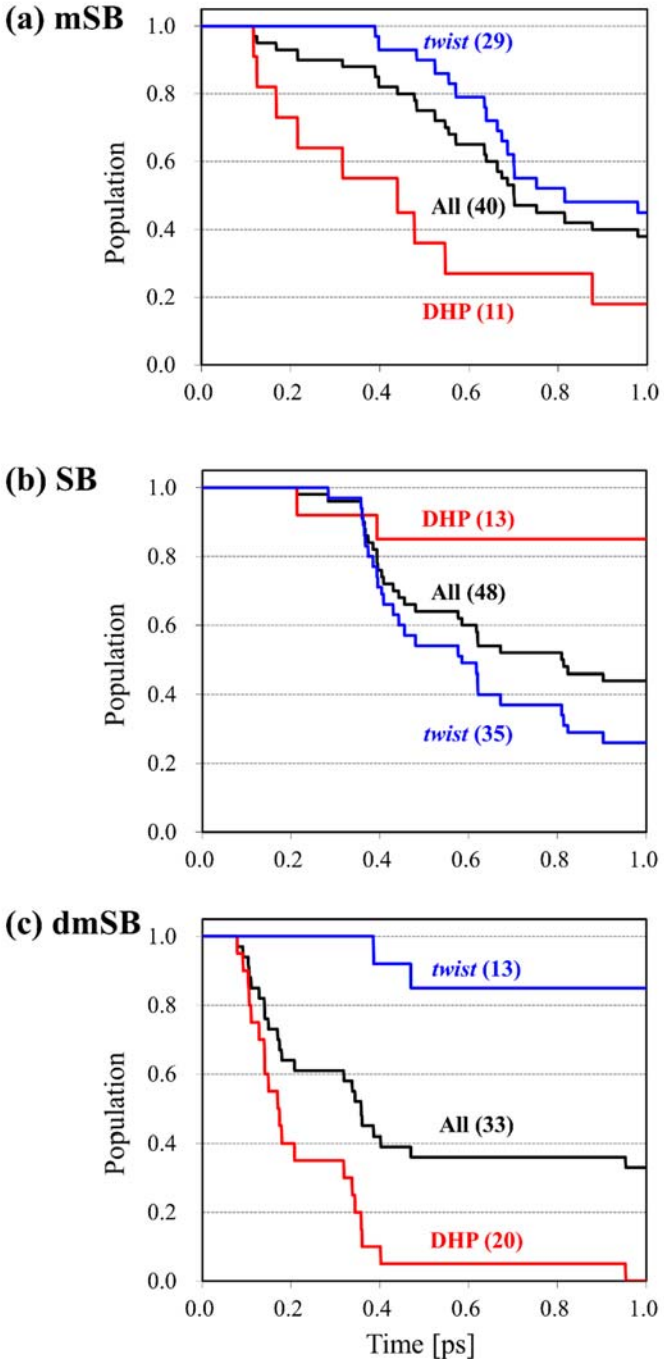

Figure 7. The decay of the S_1 population as a function of time derived from on-the-fly MD simulations for (a) *cis*-mSB, (b) *cis*-SB [31], and (c) *cis*-dmSB [39]. The S_1 population for all the trajectories is plotted in black, while the decays for the trajectories remaining in the DHP region and for those in the *twist* region are plotted in red and in blue, respectively.

IV. Conclusions

In the present study, the reaction pathways and branching dynamics on the excited-state PES for ππ*-excited *cis*-mSB were investigated by SF-TDDFT calculations and on-the-fly MD simulations, and a comparison with the previous theoretical studies on *cis*-SB [31] and *cis*-dmSB [39] has been made. In all the systems, the meta-IRC pathway starting from the FC structure of the *cis*-form is connected to the minimum in the DHP region, but the reaction path profile suggests that dynamics effects push the molecule partly to the *twist* region. In the case of *cis*-SB, all trajectories enter the *twist* region once because of the inertial force; subsequently, some trajectories enter the DHP region. In the case of *cis*-dmSB, most trajectories enter the DHP region along the meta-IRC path, and some trajectories move to the *twist* region later. The case of *cis*-mSB is intermediate between those of *cis*-SB and *cis*-dmSB, and, as the result of dynamics simulations, the branching ratio was calculated to be DHP:*twist* = 0.275:0.725, which is similar to the case of *cis*-SB. In the *twist* region, mSB hops to the ground state through the H-twisted-*trans*-pyramidal S_1/S_0-CI. Concerning S_1 population decay, *cis*-SB has a slow component assigned to trajectories terminating in the DHP region, whereas *cis*-dmSB has a slow component assigned to trajectories terminating in the *twist* region. On the other hand, *cis*-mSB has no slow component because its reaction path profile is intermediate between those of *cis*-SB and *cis*-dmSB.

Acknowledgements

This work was supported by JSPS KAKENHI with Grant Number 16KT0047 and partly supported by MEXT as "Priority Issue on Post-K computer" (Development of new fundamental technologies for high-efficiency energy creation, conversion/storage and use). YH is supported by JST for PRESTO (Grant Number JPMJPR16N8). Some of the calculations were performed using the Research Centre for Computational Science, Okazaki, Japan.

References

[1] W. Domcke, G. Stock, Theory of Ultrafast Nonadiabatic Excited-State Processes and their Spectroscopic Detection in Real Time, Advances in Chemical Physics, 1997. doi:10.1002/9780470141595.ch1.

[2] A.L. Sobolewski, W. Domcke, C. Dedonder-Lardeux, C. Jouvet, Excited-state hydrogen detachment and hydrogen transfer driven by repulsive $^1\pi\sigma^*$ states: A new paradigm for nonradiative decay in aromatic biomolecules, Phys. Chem. Chem. Phys. 4 (2002) 1093–1100. doi:10.1039/b110941n.

[3] W. Domcke, D.R. Yarkony, Role of Conical Intersections in Molecular Spectroscopy and Photoinduced Chemical Dynamics, Annu. Rev. Phys. Chem. 63 (2012) 325–352. doi:10.1146/annurev-physchem-032210-103522.

[4] S. Yamazaki, T. Taketsugu, Nonradiative Deactivation Mechanisms of Uracil, Thymine, and 5-Fluorouracil: A Comparative ab Initio Study, J. Phys. Chem. A. 116 (2012) 491–503. doi:10.1021/jp206546g.

[5] S. Yamazaki, T. Taketsugu, Photoreaction channels of the guanine–cytosine base pair explored by long-range corrected TDDFT calculations, Phys. Chem. Chem. Phys. 14 (2012) 8866. doi:10.1039/c2cp23867e.

[6] A. Nakayama, Y. Harabuchi, S. Yamazaki, T. Taketsugu, Photophysics of cytosine tautomers: new insights into the nonradiative decay mechanisms from MS-CASPT2 potential energy calculations and excited-state molecular dynamics simulations, Phys. Chem. Chem. Phys. 15 (2013) 12322. doi:10.1039/c3cp51617b.

[7] T. Taketsugu, A. Tajima, K. Ishii, T. Hirano, Ab Initio Direct Trajectory Simulation with Nonadiabatic Transitions of the Dissociative Recombination Reaction $HCNH^+ + e^- \rightarrow HNC/HCN + H$, Astrophys. J. 608 (2004) 323–329. doi:10.1086/386539.

[8] Y. Ootani, K. Satoh, A. Nakayama, T. Noro, T. Taketsugu, Ab initio molecular

dynamics simulation of photoisomerization in azobenzene in the nπ* state, J. Chem. Phys. 131 (2009) 194306. doi:10.1063/1.3263918.

[9] Y. Harabuchi, S. Maeda, T. Taketsugu, N. Minezawa, K. Morokuma, Automated Search for Minimum Energy Conical Intersection Geometries between the Lowest Two Singlet States S_0/S_1-MECIs by the Spin-Flip TDDFT Method, J. Chem. Theory Comput. 9 (2013) 4116–4123. doi:10.1021/ct400512u.

[10] S. Maeda, Y. Harabuchi, T. Taketsugu, K. Morokuma, Systematic Exploration of Minimum Energy Conical Intersection Structures near the Franck–Condon Region, J. Phys. Chem. A. 118 (2014) 12050–12058. doi:10.1021/jp507698m.

[11] S. Maeda, T. Taketsugu, K. Ohno, K. Morokuma, From Roaming Atoms to Hopping Surfaces: Mapping Out Global Reaction Routes in Photochemistry, J. Am. Chem. Soc. 137 (2015) 3433–3445. doi:10.1021/ja512394y.

[12] Y. Harabuchi, T. Taketsugu, S. Maeda, Exploration of minimum energy conical intersection structures of small polycyclic aromatic hydrocarbons: toward an understanding of the size dependence of fluorescence quantum yields, Phys. Chem. Chem. Phys. 17 (2015) 22561–22565. doi:10.1039/C5CP02103K.

[13] Y. Harabuchi, T. Taketsugu, S. Maeda, Nonadiabatic Pathways of Furan and Dibenzofuran: What Makes Dibenzofuran Fluorescent?, Chem. Lett. 45 (2016) 940–942. doi:10.1246/cl.160398.

[14] W.M. Moore, D.D. Morgan, F.R. Stermitz, The Photochemical Conversion of Stilbene to Phenanthrene. The Nature of the Intermediate, J. Am. Chem. Soc. 85 (1963) 829–830. doi:10.1021/ja00889a050.

[15] J. Saltiel, Perdeuteriostilbene. The Role of Phantom States in the cis-trans Photoisomerization of Stilbenes, J. Am. Chem. Soc. 89 (1967) 1036–1037. doi:10.1021/ja00980a057.

[16] K.A. Muszkat, E. Fischer, Structure, spectra, photochemistry, and thermal reactions of

the 4a,4b-dihydrophenanthrenes, J. Chem. Soc. B Phys. Org. (1967) 662. doi:10.1039/j29670000662.

[17] T. Wismonski-Knittel, G. Fischer, E. Fischer, Temperature dependence of photoisomerization. Part VIII. Excited-state behaviour of 1-naphthyl-2-phenyl- and 1,2-dinaphthyl-ethylenes and their photocyclisation products, and properties of the latter, J. Chem. Soc. Perkin Trans. 2. 15 (1974) 1930. doi:10.1039/p29740001930.

[18] J.A. Syage, W.R. Lambert, P.M. Felker, A.H. Zewail, R.M. Hochstrasser, Picosecond excitation and trans-cis isomerization of stilbene in a supersonic jet: Dynamics and spectra, Chem. Phys. Lett. 88 (1982) 266–270. doi:10.1016/0009-2614(82)87085-1.

[19] H. Petek, K. Yoshihara, Y. Fujiwara, Z. Lin, J.H. Penn, J.H. Frederick, Is the nonradiative decay of S1 cis-stilbene due to the dihydrophenanthrene isomerization channel? Suggestive evidence from photophysical measurements on 1,2-diphenylcycloalkenes, J. Phys. Chem. 94 (1990) 7539–7543. doi:10.1021/j100382a043.

[20] D.C. Todd, J.M. Jean, S.J. Rosenthal, A.J. Ruggiero, D. Yang, G.R. Fleming, Fluorescence upconversion study of cis-stilbene isomerization, J. Chem. Phys. 93 (1990) 8658–8668. doi:10.1063/1.459252.

[21] S. Pedersen, L. Bañares, A.H. Zewail, Femtosecond vibrational transition‐state dynamics in a chemical reaction, J. Chem. Phys. 97 (1992) 8801–8804. doi:10.1063/1.463350.

[22] J.S. Baskin, L. Bañares, S. Pedersen, A.H. Zewail, Femtosecond real-time probing of reactions. 20. Dynamics of twisting, alignment, and IVR in the trans-stilbene isomerization reaction, J. Phys. Chem. 100 (1996) 11920 –11933. doi:10.1021/jp960909x.

[23] W. Fuß, C. Kosmidis, W.E. Schmid, S.A. Trushin, The Photochemicalcis–trans Isomerization of Free Stilbene Molecules Follows a Hula-Twist Pathway, Angew. Chemie Int. Ed. 43 (2004) 4178–4182. doi:10.1002/anie.200454221.

[24] S. Takeuchi, S. Ruhman, T. Tsuneda, M. Chiba, T. Taketsugu, T. Tahara, Spectroscopic Tracking of Structural Evolution in Ultrafast Stilbene Photoisomerization, Science. 322 (2008) 1073–1077. doi:10.1126/science.1160902.

[25] T. Nakamura, S. Takeuchi, T. Taketsugu, T. Tahara, Femtosecond fluorescence study of the reaction pathways and nature of the reactive S_1 state of cis-stilbene, Phys. Chem. Chem. Phys. 14 (2012) 6225. doi:10.1039/c2cp23959k.

[26] Y. Amatatsu, Ab initio study on the electronic structures of stilbene at the conical intersection, Chem. Phys. Lett. 314 (1999) 364–368. doi:10.1016/S0009-2614(99)01042-8.

[27] V. Molina, M. Merchán, B.O. Roos, A theoretical study of the electronic spectrum of cis-stilbene, Spectrochim. Acta Part A Mol. Biomol. Spectrosc. 55 (1999) 433–446. doi:10.1016/S1386-1425(98)00252-2.

[28] J. Quenneville, T.J. Martínez, Ab Initio Study of Cis−Trans Photoisomerization in Stilbene and Ethylene, J. Phys. Chem. A. 107 (2003) 829–837. doi:10.1021/jp021210w.

[29] N. Minezawa, M.S. Gordon, Photoisomerization of Stilbene: A Spin-Flip Density Functional Theory Approach, J. Phys. Chem. A. 115 (2011) 7901–7911. doi:10.1021/jp203803a.

[30] I.N. Ioffe, A.A. Granovsky, Photoisomerization of Stilbene: The Detailed XMCQDPT2 Treatment, J. Chem. Theory Comput. 9 (2013) 4973–4990. doi:10.1021/ct400647w.

[31] Y. Harabuchi, K. Keipert, F. Zahariev, T. Taketsugu, M.S. Gordon, Dynamics Simulations with Spin-Flip Time-Dependent Density Functional Theory: Photoisomerization and Photocyclization Mechanisms of cis- Stilbene in $\pi\pi^*$ States, J. Phys. Chem. A. 118 (2014) 11987–11998. doi:10.1021/jp5072428.

[32] T. Taketsugu, Y. Harabuchi, Ab Initio Molecular Dynamics Study on Photoisomerization Reactions: Applications to Azobenzene and Stilbene, Frontiers of

Quantum Chemistry, Springer Singapore, 2018. doi:10.1007/978-981-10-5651-2_18.

[33] Y. Shao, M. Head-Gordon, A.I. Krylov, The spin–flip approach within time-dependent density functional theory: Theory and applications to diradicals, J. Chem. Phys. 118 (2003) 4807–4818. doi:10.1063/1.1545679.

[34] F. Wang, T. Ziegler, Time-dependent density functional theory based on a noncollinear formulation of the exchange-correlation potential, J. Chem. Phys. 121 (2004) 12191. doi:10.1063/1.1821494.

[35] N. Minezawa, M.S. Gordon, Optimizing Conical Intersections by Spin−Flip Density Functional Theory: Application to Ethylene, J. Phys. Chem. A. 113 (2009) 12749–12753. doi:10.1021/jp908032x.

[36] S. Maeda, Y. Harabuchi, Y. Ono, T. Taketsugu, K. Morokuma, Intrinsic reaction coordinate: Calculation, bifurcation, and automated search, Int. J. Quantum Chem. 115 (2015) 258–269. doi:10.1002/qua.24757.

[37] T. Tsutsumi, Y. Harabuchi, Y. Ono, S. Maeda, T. Taketsugu, Analyses of trajectory on-the-fly based on the global reaction route map, Phys. Chem. Chem. Phys. 20 (2018) 1364–1372. doi:10.1039/C7CP06528K.

[38] F. Berndt, A.L. Dobryakov, M. Quick, R. Mahrwald, N.P. Ernsting, D. Lenoir, S.A. Kovalenko, Long-lived perpendicular conformation in the photoisomerization path of 1,1′-dimethylstilbene and 1,1′-diethylstilbene, Chem. Phys. Lett. 544 (2012) 39–42. doi:10.1016/j.cplett.2012.07.007.

[39] Y. Harabuchi, R. Yamamoto, S. Maeda, S. Takeuchi, T. Tahara, T. Taketsugu, Ab Initio Molecular Dynamics Study of the Photoreaction of 1,1′-Dimethylstilbene upon $S_0 \rightarrow S_1$ Excitation, J. Phys. Chem. A. 120 (2016) 8804–8812. doi:10.1021/acs.jpca.6b07548.

[40] K. Kokado, T. Machida, T. Iwasa, T. Taketsugu, K. Sada, Twist of C═C Bond Plays a Crucial Role in the Quenching of AIE-Active Tetraphenylethene Derivatives in

Solution, J. Phys. Chem. C. 122 (2018) 245–251. doi:10.1021/acs.jpcc.7b11248.

[41] M.W. Schmidt, K.K. Baldridge, J.A. Boatz, S.T. Elbert, M.S. Gordon, J.H. Jensen, S. Koseki, N. Matsunaga, K.A. Nguyen, S. Su, T.L. Windus, M. Dupuis, J.A. Montgomery, General atomic and molecular electronic structure system, J. Comput. Chem. 14 (1993) 1347–1363. doi:10.1002/jcc.540141112.

[42] S. Maeda, Y. Harabuchi, Y. Sumiya, M. Takagi, M. Hatanaka, Y. Osada, T. Taketsugu, K. Morokuma, K. Ohno, GRRM (a developmental version). Hokkaido University, Sapporo, Japan 2017, see http://grrm.chem.tohoku.ac.jp/GRRM/index_e.html, accessed on March 3, 2016.

[43] S. Maeda, K. Ohno, K. Morokuma, Updated Branching Plane for Finding Conical Intersections without Coupling Derivative Vectors, J. Chem. Theory Comput. 6 (2010) 1538–1545. doi:10.1021/ct1000268.

[44] Y. Harabuchi, M. Okai, R. Yamamoto, T. Tsutsumi, Y. Ono, T. Taketsugu, SPPR, a developmental version. Hokkaido University, Sapporo, Japan 2018.